

# Correlated photonic qutrit pairs for quantum information and communication

Debadrita Ghosh<sup>1</sup>, Thomas Jennewein<sup>2,3</sup>, Piotr Kolenderski<sup>4</sup>, and Urbasi Sinha<sup>\*1</sup>

<sup>1</sup>*Raman Research Institute, Sadashivanagar, Bengaluru 560080, India*

<sup>2</sup>*Institute for Quantum Computing, University of Waterloo,*

*200 University Avenue West, Waterloo, Ontario N2L3G1, Canada*

<sup>3</sup>*Department of Physics and Astronomy, University of Waterloo, Waterloo, Ontario, Canada and*

<sup>4</sup>*Faculty of Physics, Astronomy and Informatics,*

*Nicolaus Copernicus University, Grudziadzka 5, 87-100 Toruń, Poland\**

(Dated: Compiled February 10, 2017)

Higher dimensional quantum systems have a very important role to play in quantum information, computation as well as communication. In photonic systems, it is common to use the photon's polarization degree of freedom for various investigations. However, this restricts us to only two orthogonal states, hence qubits for manipulation. In this paper, we have theoretically analysed and experimentally demonstrated a system of two photonic qutrits which are correlated in the spatial degree of freedom. The qutrits have been generated by modulating the pump beam in a spontaneous parametric down conversion process using an aperture based system. In principle, this system can be scaled up to generation of even higher dimensional correlated qudits with possible application for quantum communication and computation implementations.

## I. INTRODUCTION

The ability to generate and detect correlated photon pairs by means of spontaneous parametric down conversion (SPDC) offers lots of experimental possibilities ranging from fundamental tests of quantum theory [1] to practical applications in quantum information [2] and quantum communication [3]. The influence of the pump beam spatial mode on the characteristics of the resulting photon pairs has been analyzed in terms of optimization of the collecting of the photon pairs in single mode fibres [4]. Recently it was analysed how the pump beam spatial mode influences the spatial characteristics of the resulting photon pairs [3]. In the Ref. [5] the authors analyze the case where the pump beam is prepared in Bessel-Gauss mode. In turn, Pugh *et al* [3] show the way to control the pump beam for the application for long distance quantum communication with satellites.

Along these lines, there is an extensive research towards encoding of quantum information in a single photon's degree of freedom. Spatial degree of freedom offers a variety of possibilities such as orbital angular momentum [6, 7] or spatial qudits [8–10]. The latter framework proved to be useful when testing fundamentals of quantum theory [11–13]. In earlier work [12], it has been shown that a triple slit aperture placed in the path of a photon leads to the generation of a spatial qutrit. Note that in practice the transmission of the system, which is fundamentally very low, limits the robustness in terms of counting rates. The use of calcite beam displacer can reduce this problem for a qubit implementation [14, 15]. However the scaling towards higher dimensional states is challenging within this framework.

Here we assume that the pump beam is prepared such that its spatial mode resembles three slits. By thus imprinting the pump beam with a triple slit profile, we investigate if this spatial structure is also carried through

faithfully to the resultant signal and idler photons. We then investigate the correlations that exist between the signal and idler photons in the spatial domain and effectively generate spatially correlated qutrits with a Pearson coefficient as high as 90 percent.

In this work, we modulate the pump beam itself to generate a spatially correlated pair of qutrits. The question we ask is whether the simple slit-like correlation can be preserved in the process of SPDC and we find very convincing match between theoretical predictions and experimental results. We also lay down the recipe for the optimal choice of experimental parameters which can be exploited in future architecture to maximize the correlations.

## II. TRIPLE-SLIT-BASED QUTRITS

Let us consider a setup depicted in Fig. 1 consisting of a Type I non-linear crystal. We are using the collinear geometry for our down conversion process. The pump beam spatial mode is prepared by transferring a gaussian beam through a set of three slits (centred at the middle slit) and imaging the result on the crystal using a lens in the 2f - 2f configuration.

While we have theoretically worked out the detailed image transfer formulation for our system (which we discuss in the appendix), we have used three box functions weighted by a Gaussian as the pump profile in the crystal to generate the bi-photon qutrits and their resultant correlations so that the simulations ended in finite time.

We have followed [16] to solve for phase matching in the Type I SPDC process. The crystal that we have used is BBO with a cut angle of 29.3° for non collinear SPDC process. For type I SPDC, we define the phase mismatch as

$$\Delta \vec{k} = \vec{k}_p(\omega_p, \alpha, n_e(\theta)) - \vec{k}_s(\omega_s, \alpha, n_o) - \vec{k}_i(\omega_i, \alpha, n_o). \quad (1)$$

\*Electronic address: usinha@rri.res.in

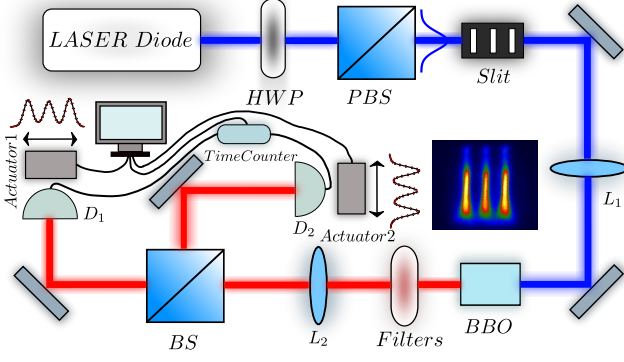


FIG. 1: Experimental setup.

Here,  $\omega_p, \omega_s$  and  $\omega_i$  refer to the frequency of the pump, signal and idler photons respectively, and  $n_e$  and  $n_o$  refer to extraordinary and ordinary refractive indices. The pump wave vector inside the crystal depends on the angle  $\alpha$  it makes with the crystal cut.

The SPDC process considered here is  $e \rightarrow oo$ . For collinear degenerate SPDC, we expect  $\vec{\Delta k} = 0$ . Using parameters of refractive index from BBO Sellmeier equations, we have the collinear phase matching at  $28.81^\circ$ .

Given a phase mismatch  $\Delta \vec{k}$ , we assign the intensity weight to it as

$$|\text{sinc}(\Delta k_x L_x) \text{sinc}(\Delta k_z L_z)|^2, \quad (2)$$

where  $L_x$  is the transverse length of the crystal and  $L_z$  is the thickness of the crystal along beam propagation direction. We have ignored the transverse length along the height i.e. y-axis for ease of computation.

Following [16, 17], we can find the Hamiltonian for the SPDC process where the pump is treated classically and the signal and idler are treated as perturbations. For degenerate down-conversion  $\omega_p = 2\omega_s = 2\omega_i$  and the probability amplitude to get a coincidence for degenerate photons generated from collinear SPDC will be:

$$\mathcal{A} \propto \int_V d^3r \int dk_s \int dk_i A_p(x, y, z) \exp(i(\vec{k}_p - \vec{k}_s - \vec{k}_i) \cdot \vec{r}) \quad (3)$$

Here,  $A_p(x, y, z)$  is the amplitude of the pump as a function of space.  $z$  is assumed to be the direction of propagation of pump,  $\vec{k}_p, \vec{k}_s$  and  $\vec{k}_i$  are the pump, signal and idler wave vectors respectively. The integral over  $dk_s$  depends on the angle that the detector subtends to the crystal. For point detectors we have a single value of  $\vec{k}_{s,i}$ . However, the limits of integration for finite sized detectors for the  $\vec{k}_s$  will be of the form  $\vec{k}_s^\mu \pm \vec{k}_s^\Delta$ . Here  $\vec{k}_s^\mu$  is determined by the position of the detectors and  $\vec{k}_s^\Delta$  is determined by the size of the detectors.

We now attempt to compute  $\mathcal{A}$  numerically. However, integration of the complex exponential is numerically cumbersome and does not converge. Hence we assume that  $\vec{k}_p$  does not depend on position inside the crystal, so that we can integrate the exponential independently and replace it with a sinc function.

We use the approximation

$$\mathcal{A}(k_s, k_i) = \int_V d^3r A_p(x, y, z) \Pi_{i=x,y,z} \text{sinc}(\Delta k_i(\Delta r) L_i) \quad (4)$$

Here  $\Pi_{i=x,y,z} \text{sinc}(\Delta k_i(r) L_i)$  should be interpreted as the weight associated with a point classical pump and here the phase matching is weighted by the length of the crystal. Then we consider that the pump is composed of several such point pumps and we assume that different points in the crystal are independent as far as wave vectors are considered. Note that phase mismatch depends on  $\Delta r$ , the difference between crystal and detector positions (and not just on the crystal position).

In the simulation code, we integrate over two coordinates (x and z). We are interested in the transverse correlation (along x). The height of the slit is assumed to be infinity, pump wave vector is assumed to be along z-direction only, assuming a thin crystal and each point in the crystal is assumed to have SPDC independently with the weight  $\text{sinc}(\Delta k_i(\Delta r) L_i)$ .

We follow the following algorithm to compute  $|\mathcal{A}(k_s, k_i)|^2$ .

- Compute  $\Delta k$  for a pair of signal and idler points and for a given point on the crystal.
- Compute the point to point correlation as the product of intensity of the pump at the given crystal point  $|A_p|^2$  and the weight function  $|\Pi_{i=x,y,z} \text{sinc}(\Delta k_i(r) L_i)|^2$
- Integrate over the signal/idler position about the mean detector position and with range equal to the size of detector.
- Repeat the above for different idler points to get the spatial correlation between a signal position and the entire idler profile.
- Sum the idler profile computed for different signal positions to get the signal profile. We moved the signal detector with a step size of  $3\mu\text{m}$  to attain convergence in this code.

The choice of detector plane after the crystal was given due consideration and is discussed in the appendix.

The above simulations were carried out for different choice of simulation parameters to obtain an optimal set of parameters that gives us a high value of Pearson correlation coefficient [18]. In these simulations, we have assumed point detectors to enable faster simulations. In the result of the numerical simulation we get an approximation of the probability distribution of the coincidence detection of signal photon at position  $x_1$  and idler photon at position  $x_2$ . Based on the numerical data one can easily compute correlation coefficient as a ratio of covariance over a product of respective variances for signal and idler photon detector positions:  $r = \langle x_1 x_2 \rangle / \sqrt{\langle x_1^2 \rangle \langle x_2^2 \rangle}$ .

We have done the above simulations for both Type I and Type II SPDC using the same crystal, lens and

$w$ in $\mu m$	$d$ in $\mu m$	$L_z$ in mm	Pearson coefficient
30	50	10	0.872393
30	100	10	0.965584
30	200	10	0.992088
5	100	10	0.964352
10	100	10	0.966075
30	100	10	0.965584
40	100	10	0.966569
30	100	5	0.929685
30	100	10	0.965584
30	100	100	0.998688

TABLE I: Table comparing the Pearson coefficients varying slit width  $w$ , inter-slit distance  $d$ , crystal longitudinal length  $L_z$  respectively.

slit parameters and found that the Pearson coefficient for Type II process is 0.985(2) whereas for Type I, it is 0.966(2). We still decided to design an experiment using a Type I crystal as we were concerned that transverse walk off which could happen to one of the two orthogonal polarizations exhibited by signal and idler photons could mask the otherwise high correlations that have been predicted from theory.

We have chosen the triple slit system to have slit width of  $30\mu m$ , inter-slit distance of  $100\mu m$ , slit height of  $300\mu m$ . For this, we have chosen an incident pump beam with a Gaussian RMS width of  $300\mu m$ . This is an optimal choice as we wish to strike a balance between throughput and uniform distribution. For a wider beam width, the number of singles and coincidence counts is expected to drop significantly whereas a smaller beam width would result in the three slits not all being centred close to the peak of the Gaussian.

We have done the simulations for each of the slit parameters keeping other parameters constant and ascertained that the Pearson coefficient is high for our final choice. Table 1 shows the comparison between different slit and crystal parameters in terms of the Pearson coefficient. Further details of these parameter optimization simulations are discussed in the Appendix.

### III. EXPERIMENT

The Type I BBO crystal is cut for non-collinear phase matching at 405 nm to  $2 \times 810$  nm at  $29.3^\circ$  which translates to collinear phase matching at  $28.8^\circ$ . The parameter of the slits and pump beam are as mentioned above and the focal length of the lens performing image transfer from slit plane to centre of non linear crystal is  $146mm$  for blue incident beam. The focal length of the lens performing the image transfer of the signal and idler photons to the detector plane is  $150mm$  for IR wavelength.

The detectors D1 (D2) are mounted on motorized

stages (ZST225B and ZST213 from Thorlabs respectively) allowing control of their position in the plane orthogonal to the propagation of signal (idler) photon. The accuracy of the motors is sub micron level. We measured single counts and coincidences of detection at both detectors with a coincidence time window of 1024 ps using FPGA electronics (UQD LOGIC-16). We scanned the characteristic range in the direction orthogonal to the slits' longer dimension with both the detectors. While one of the detectors (D1) scanned the signal photon spatial profile, D2 scanned the idler photon profile. By keeping D1 fixed at different positions of the signal profile, we scanned the detector D2 to yield correlations between the signal position and the entire idler profile. We decided on 13 fixed detector positions for sufficient statistics. These 13 positions correspond to peaks, dips and asymmetrically chosen slope positions to give us maximum information as per a Nyquist sampling criterion. For each D1 fixed position, D2 was moved with a step size of  $10\mu m$ . The data acquisition time was 180 sec at each point, resulting in one complete D2 run taking close to three hours. We repeat the measurement 5 times for better averaging. Thus, for each fixed signal position, we take close to 15 hours to generate the idler profile and resultant correlations.

### IV. RESULTS

The result of coincidence counting is plotted in Fig. 2(a). The experimental correlations between signal and idler positions are appropriately captured by the measurement of coincidences. For the measure of correlation we take the Pearson's coefficient. Here the random variables are detectors' positions,  $x_1$  and  $x_2$  and the probability distribution is estimated directly by our measurement. The probability of getting a coincidence detection at positions  $x_1$  and  $x_2$  is proportional to the coincidence counts measured and depicted in Fig. 2(a). The estimate of the Pearson's correlation coefficient is  $-0.902(2)$ . We estimated the uncertainty of the coefficient by simulating  $10^5$  probability distributions based on the measured statistics and assuming Poisson statistics of the counts.

Red dots in Fig. 2(b), (c) and (d) correspond to coincidences  $R_c$  measured as the idler detector is moved while the signal detector is kept fixed at first peak (slit A), second peak (slit B) and third peak (slit C) respectively. Error bars for both position and number uncertainty have been included. The blue lines represent the theoretically simulated correlation profiles.

There are three ways in which one can generate the commensurate theory graphs with respect to the modelling of the pump profile at the crystal. Two methods have already been discussed above which involve using a detailed image transfer formalism or using three box functions weighted by a Gaussian. In order to capture the correlations due to the actual pump beam profile that has been transferred to the crystal, we measured the pump beam profile that is transferred to the position of the centre of the crystal using a lens in 2f-2f configu-

ration and used this profile itself to generate the signal and idler profiles as well as calculating the spatial correlations between the two profiles. Slight difference in manifestation between the experimental and theoretically simulated profiles has been accounted for in the simulations. An example of a pump beam profile at the crystal position is given in the appendix. The use of the experimentally measured pump profile to generate the correlation has the advantage that any non-idealness that may exist in the experiment in terms of alignment or otherwise would then be captured in the theory and the comparison would not suffer from comparing experimental data with ideal theory conditions.

While Fig. 2(a) shows  $R_c$  for all measured detector positions, in Fig. 2(b), (c) and (d), we have chosen to highlight the correlations at the peak positions in a 2-D format to enable representation of the error bars in terms of position and number uncertainty and also indicate the extent of overlap between theoretical predictions and experimental results. Fig. 2(e) shows the comparison between the single photon counts  $R_s$  measured as a function of detector position for the signal photon and the theoretically generated profile. Experimental and theoretically generated  $R_c$  and  $R_s$  have been appropriately normalized by their respective maxima.

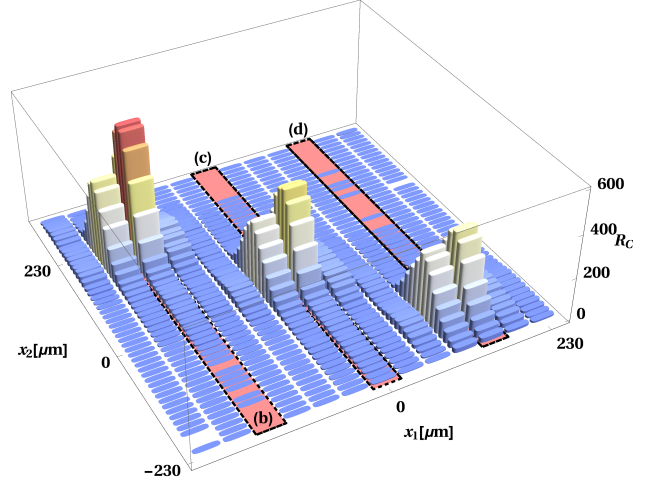
The slit B is physically slightly thinner than the other two slits in manufacture, hence the number of single photons measured when the detector is placed at slit B position is slightly less than those measured at slit positions A and C. By choosing to perform the theoretical analysis using the experimentally measured pump as a starting point, we see that the single photons generated from down conversion almost perfectly carry the pump profile through as a result of which there is remarkable agreement between theory and experiment. In Fig. 2(b), (c) and (d), we find that as expected the theory captures the slight difference in sizes of the slits wherein peaks of slits A and C show higher  $R_C$  than slit B. In the experimental plots, we find that while indeed  $R_C$  for C is higher than B, the one for A is slightly lower than B which can be ascribed to slight difference in performance of the actuators that are controlling the individual detector movements. While the  $R_s$  is generated with a single detector (D1) motion,  $R_C$  involves both detectors.

## V. DISCUSSION/OUTLOOK

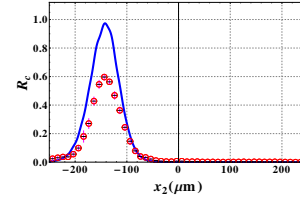
The presented results show that it is possible to generate photon pairs with intrinsic spatial correlation. This can be used for implementation of quantum information protocols which require higher dimensional quantum systems. It is possible to encode a qutrit using a system of three slits similarly as in the Ref. [12], but in the present case, one can have access to two correlated qutrits by modulating the pump profile.

This may prove to be a means to generate higher dimensional entanglement paving a possible route towards quantum communication and information processing using novel higher dimensional entangled photon states.

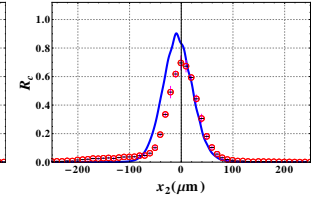
(a) Coincidence map



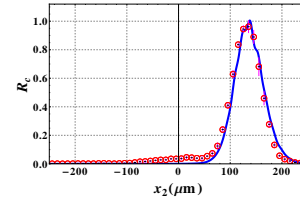
(b) D1 at the slit A, D2 moving



(c) D1 at the slit B, D2 moving



(d) D1 at the slit C, D2 moving



(e) D1 moving

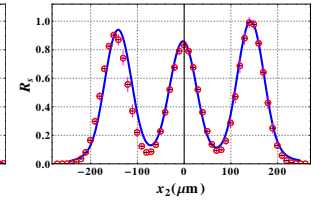


FIG. 2: (a) Coincidence counts,  $R_C$  measured as a function of position of detectors D1 and D2. A comparison between experimental and theoretically predicted coincidence counts when detector D1 is fixed at peaks of slit (b) A, (c) B, (d) C and the detector D2 is scanning. (e) Single counts,  $R_s$  measured at detector D1. Each data point has a measurement time of 3 minutes.

## Acknowledgements

We acknowledge Eneet Kaur for assistance in initial calculations and especially S.N.Sahoo for technical assistance and his generous help during various stages of the project. PK acknowledges support by the National Laboratory of Atomic, Molecular and Optical Physics, Torun, Poland, and Fundacja na rzecz Nauki Polskiej (FNP) (Homing Plus grant no. 2013-7/9) and Ministerstwo Nauki i Szkolnictwa Wzszego (MNiSW) (Iuventus Plus grant no. IP2014 020873, grant no. 6576/IA/SP/2016).

## Appendix A: Image transfer formalism

There are certain assumptions which go into the image transfer formulation. All calculations are done in two dimensions which are the beam propagation direction "z" and the transverse "x" direction. We are assuming that the slit height can be approximated to be infinitely long compared to the slit width. Scalar field paraxial approximations for a thin lens are used. The centre of the crystal is assumed to be perfectly at twice the focal length from the lens.

The system of lenses and mirrors transfers the image of the slits to the crystal. The center of the crystal is at 2f from the thin lens. Its transfer function is given by:

$$H(x_i, z_i; x_o, z_o) = \int_{-R}^R \frac{e^{\frac{1}{2} \frac{ikx_o^2}{z_o}} e^{\frac{1}{2} ik \left( \frac{1}{z_o} + \frac{1}{z_i} - \frac{1}{f} \right) x_l^2} e^{-ik \left( \frac{x_o}{z_o} + \frac{x_i}{z_i} \right) x_l}}{\lambda^2 z_o z_i} dx_l. \quad (A1)$$

Here  $(x_o, z_o)$  are the coordinates of the object whose image is to be transferred to a location  $(x_i, z_i)$  and  $\lambda$  is the wavelength of the incident beam. Thus, in order to transfer the scalar field  $U(x_o; z_o)$  to  $U(x_i; z_i)$ , we would use the following transformation equation and the scalar field after the lens would then be given as:

$$U(x_i; z_i) = \int_{-\infty}^{\infty} dx_o U(x_o; z_o) H(x_i, z_i; x_o, z_o) \quad (A2)$$

It yields the image transferred at crystal position. The integration in (A1) is done analytically whereas the final integration in (A2) is evaluated by numerical means using *Mathematica 11*. Thus instead of using uniform top hat functions as representations of the slit profiles, we have used the lens transfer formulation to transfer the image of the slits to the centre of the crystal when the slits are illuminated by a Gaussian.

## Appendix B: Choice of detector plane

The choice of detector plane after the crystal was given due consideration. After investigating options to place the detector directly after the crystal, at the focus of another lens after the crystal as well as in the far field, we came up with the optimal arrangement in which another lens is used in the 2f-2f configuration after the crystal to detect signal and idler photons that carry the image of the pump profile (which itself was transferred through a separate lens in the 2f-2f configuration on the crystal). However, we were unable to simulate a second lens after the crystal due to complexity of the integrand. Instead of a second lens, we would need to place the detectors right after the crystal in the simulation. Placing the detectors far away from the crystal would entail generating an interference pattern. From a very large distance, the angles subtended by detectors to the individual slits would be almost the same and hence we would end up collecting photons from all three slit illuminations. We have the

weights associated as  $\text{Sinc}(\Delta k_x(x_c)L_x)$ . Now when the detectors are too close or inside the crystal, the angle subtended by the detector to any crystal point would be very large and as a consequence the phase match will be large and the integrand will be very highly oscillatory resulting in numerical errors. Hence we decided to place the detector at 1mm from the front surface of the crystal which gave us reasonable theoretical expectations.

## Appendix C: Simulations to determine the optimal set of parameters for high resultant spatial correlations

First, we varied the slit width keeping other parameters constant. For slit widths ranging from  $5\mu\text{m}$  to  $40\mu\text{m}$ , the Pearson coefficient remained around 0.96 which indicates that for these conditions, choosing a slit width in the above range should be sufficient. We decided to choose  $30\mu\text{m}$ . Next, we varied the inter-slit distance from  $50\mu\text{m}$  to  $200\mu\text{m}$ . The Pearson coefficient is found to increase with increasing distance between the slits kept at a constant slit width. This is perfectly in synchronization with intuition which dictates that as the slits are more separated, the overlap between them goes down, as a result of which the point to point correlation increases. However, a  $200\mu\text{m}$  interslit distance would entail a much bigger incident pump beam which could again lead to less throughput so we decided to choose the  $100\mu\text{m}$  interslit distance as a compromise between throughput and correlation coefficient. Before choosing the crystal length, we also simulated for different crystal lengths keeping slit and beam parameters constant. If we consider the intensity weight function associated with phase matching, we have along the longitudinal axis  $\text{sinc}(\Delta k_z \times L_z/2)$ . As  $L_z$  increases the sinc function becomes narrower as a result of which SPDC with large phase mismatch does not occur and the correlation becomes sharper. This was substantiated by the simulations which showed a steady increase in Pearson coefficient as crystal length was increased from  $5\text{mm}$  to  $100\text{mm}$ . However, as we wish to transfer the image of the slits to the centre of the crystal, having too long a crystal would mean that various portions of the crystal would be illuminated by the interference pattern instead, notwithstanding prohibitive cost of crystal. Too short a crystal would have low correlation coefficients. Thus, we selected a crystal length which is not too long but also yields an expected high correlation coefficient i.e.  $10\text{mm}$ . The transverse length of the crystal needs to be larger than the extent of the transverse pump profile and was chosen to be  $5\text{mm}$ .

## Appendix D: Comparison between experimental and theoretical triple slit image transfer

Figure 3 shows an example of the image transferred to the centre of the crystal comparing experimentally obtained images with theoretically simulated ones with a triple slit modulated pump profile. Figure on left shows

the image as a function of position in the crystal along beam propagation direction.

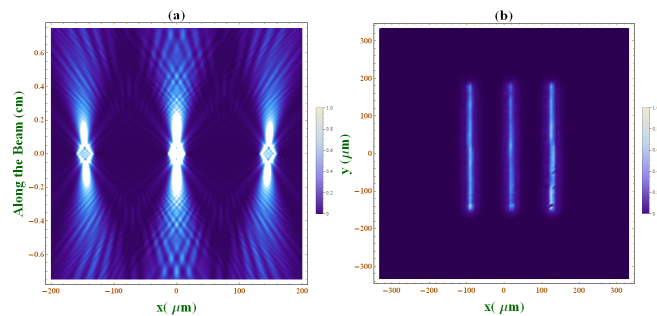


FIG. 3: Figure on left shows the theoretically simulated pump profile. When the lens is used for image transfer experimentally, a magnification is introduced in the system, which has also been incorporated in theory. While the y-axis denotes the crystal length along beam propagation direction, the x-axis denotes the image along the transverse crystal direction. The figure on the right is the experimentally measured image of the modulated pump at the position corresponding to centre of the crystal using a lens.

- [1] U. Sinha, C. Couteau, T. Jennewein, R. Laflamme, and G. Weihs, *Science* **329**, 418 (2010).
- [2] M. A. Nielsen and I. L. Chuang, *Quantum Computation and Quantum Information*, 1st ed. (Cambridge University Press, 2000).
- [3] C. J. Pugh, P. Kolenderski, C. Scarcella, A. Tosi, and T. Jennewein, *Opt. Express* **24**, 20947 (2016), 1606.04110 .
- [4] A. Gajewski and P. Kolenderski, *Phys. Rev. A* **94**, 013838 (2016).
- [5] V. Vicuña-Hernández, J. T. Santiago, Y. Jerónimo-Moreno, R. Ramírez-Alarcón, H. Cruz-Ramírez, A. B. URen, and R. Jáuregui-Renaud, *Phys. Rev. A* **94** (2016), 10.1103/physreva.94.063863.
- [6] A. Mair, A. Vaziri, G. Weihs, and A. Zeilinger, *Nature* **412**, 313 (2001).
- [7] G. Molina-Terriza, J. P. Torres, and L. Torner, *Nat Phys* **3**, 305 (2007).
- [8] L. Neves, S. Pádúa, and C. Saavedra, *Phys. Rev. A* **69**, 042305 (2004).
- [9] L. Neves, G. Lima, J. G. Aguirre Gómez, C. H. Monken, C. Saavedra, and S. Pádúa, *Phys. Rev. Lett.* **94**, 100501 (2005), arXiv:quant-ph/0411054 .
- [10] L. Neves, G. Lima, E. J. S. Fonseca, L. Davidovich, and S. Pádúa, *Phys. Rev. A* **76**, 032314 (2007).
- [11] A. Sinha, A. H. Vijay, and U. Sinha, *Sci. Rep.* **5**, 10304 (2015), 1412.2198 .
- [12] P. Kolenderski, U. Sinha, L. Youning, T. Zhao, M. Volpini, A. Cabello, R. Laflamme, and T. Jennewein, *Phys. Rev. A* **86**, 012321 (2012), arXiv:1107.5828 .
- [13] R. Sawant, J. Samuel, A. Sinha, S. Sinha, and U. Sinha, *Phys. Rev. Lett.* **113** (2014), 10.1103/physrevlett.113.120406.
- [14] P. Kolenderski, C. Scarcella, K. D. Johnsen, D. R. Hamel, C. Holloway, L. K. Shalm, S. Tisa, A. Tosi, K. J. Resch, and T. Jennewein, *Sci. Rep.* **4**, 4685 (2014).
- [15] P. Kolenderski, K. D. Johnsen, C. Scarcella, D. Hamel, K. Shalm, S. Bellisai, A. Tosi, K. Resch, and T. Jennewein, “Experimental state estimation using 28-element quantum measurement,” (2014), (in preparation).
- [16] N. Boeuf, D. Branning, I. Chaperot, E. Dauler, S. Guerin, G. Jaeger, A. Muller, and A. L. Migdall, *Opt. Eng.* **39**, 1016 (2000).
- [17] P. Kolenderski, W. Wasilewski, and K. Banaszek, *Phys. Rev. A* **80**, 013811 (2009), arXiv:0905.0009 .
- [18] K. Pearson, *Proceedings of the Royal Society of London* **58**, 240242 (1895).